International Journal of Naval Architecture and Ocean Engineering 13 (2021) 554–565

Contents lists available at ScienceDirect

International Journal of Naval Architecture and Ocean Engineering

journal homepage: http://www.journals.elsevier.com/international-journal-of-naval-architecture-and-ocean-engineering/

Bubble formation in globe valve and flow characteristics of partially filled pipe water flow

Quang Khai Nguyen [a], Kwang Hyo Jung [a, *], Gang Nam Lee [a], Hyun Jung Park [a], Peter To [b], Sung Bu Suh [c], Jaeyong Lee [c]

[a] Department of Naval Architecture and Ocean Engineering, Pusan National University, Busan, Republic of Korea
[b] College of Science & Engineering, James Cook University, Townsville, QLD, Australia
[c] Department of Naval Architecture and Ocean Engineering, Dong-Eui University, Busan, Republic of Korea

ARTICLE INFO

Article history:
Received 15 April 2021
Accepted 24 June 2021
Available online 30 June 2021

Keywords:
Globe valve
Flow coefficient
Water fraction
Pressure fluctuation
Bubble formation
Aerated flow

ABSTRACT

Air bubble entrainment is a phenomenon that can significantly reduce the efficiency of liquid motion in piping systems. In the present study, the bubble formation mechanism in a globe valve with 90% water fraction flow is explained by visualization study and pressure oscillation analysis. The shadowgraph imaging technique is applied to illustrate the unsteady flow inside the transparent valve. This helps to study the effect of bubbles induced by the globe valve on pressure distribution and valve flow coefficient. International Society of Automation (ISA) recommends locations for measuring pressure drop of the valve to determine its flow coefficient. This paper presents the comparison of the pressures at different locations along with the upstream and the downstream of the valve with the values at recommended positions by the ISA standard. The results show that in partially filled pipe flow, the discrepancies in pressure between different measurement locations in the valve downstream are significant at valve openings less than 30%. The aerated flow induces the oscillation in pressure and flow rate, which leads to the fluctuation in the flow coefficient of the valve. The flow coefficients have a linear relationship with the Reynolds number. For the same increase of Reynolds number, the flow coefficients grow faster with larger valve openings and level off at the opening of 50%.

1. Introduction

Globe valves are used in various industrial applications including offshore pipelines and oil and gas refineries. Although sizing a valve and predicting its pressure drop with single-phase flow is a straightforward task, more challenges are faced with two-phase flow due to its complex flow condition.

The hydraulic devices are characterized by several coefficients. The flow coefficient is associated with the performance of a control valve, but a safety relief valve is classified by its discharge coefficient. In order to provide the reference for evaluating the hydraulic performance of the valve, the International Society of Automation (ISA, Durham, N.C., USA) recommended standards with equations and applying conditions for a proper calculation of the flow coefficient and introduced factors to modify the formulas in various operating and testing conditions (ISA, 1972; ISA, 2012). Based on the recommendation of the ISA standard, Rahmeyer and Driskell (1985) investigated the flow coefficient of gate and butterfly control valves and concluded that the calculation of flow coefficients should use pressure taps located at 1D (nominal diameter) upstream and 10D downstream of the valve. Davis and Stewart (2002a, 2002b) used an axisymmetric numerical model to predict the flow coefficient of the globe control valve and were experimentally validated. They observed that the simulation results matched well with experiments up to 60% of valve opening. For higher openings, the flow field could change from an axisymmetric flow field to a three-dimensional one which decreased the accuracy of the numerical model. Based on experimental data with calculation determined by ISA standard, Grace and Frawley (2011) presented parametric equations to predict the valve coefficient for choke valves. They recommended that the equation gave good estimates of the valve coefficient for new valve trim designs with a 5% difference from experimental results. Ferreira et al. (2018) described the loss coefficient of the ball valve as a function of the

* Corresponding author.
E-mail address: kjung@pusan.ac.kr (K.H. Jung).
Peer review under responsibility of Society of Naval Architects of Korea.

https://doi.org/10.1016/j.ijnaoe.2021.06.007

Reynolds number. They tested a ball valve in a pressurized pipe system under steady conditions and showed that the response of the valve depends on the valve geometry, valve opening, and flow regime. Nguyen et al. (2020) studied pressure distribution and flow coefficient of globe valve with a series of experiments conducted in a flow test loop. The results showed that the flow coefficients level off when the Reynolds number exceeds a certain value.

Nevertheless, there is a limited number of studies on the globe valves with Partially Filled Pipe Flow (PFPF), which often occurs in numerous piping systems. In general, high oscillation flow characteristics produce a high vibration on pipes that leads to crack and corrosion of the pipes. Henry et al. (2018) discussed various phenomena in a horizontal PFPF using stereoscopic particle imaging velocimetry. They investigated the pressure-driven laminar and turbulent flows and found out that the friction factor is a function of Reynolds number and Froude number. They also revealed that the motions in PFPF are compressed and distorted by the existence of the free surface and mean secondary motion. Ng et al. (2001) used the Boundary Element Method (BEM) to evaluate the volumetric flow rate, the wall shear stress, and the velocity profiles of gravity-driven laminar flow in a partially filled pipe. They concluded that with the BEM, only three physical parameters, the Bond number, the contact angle, and the holdup of the free surface are required to describe the flow system. A visualization study was applied to investigate the heat transfer in a PFPF (Chatterjee et al., 2017). In that work, thermal imaging was used to capture outer wall temperature to provide an insight into the single-phase heat transfer characteristics of a rotating heated pipe. The flow transitions in PFPF were also studied by Chatterjee et al. (2018). They investigated the effects of liquid flow rate, pipe inclination, diameter, and length on the flow transitions. The study developed a flow regime map based on Reynolds number and Froude number to undertake parametric study for fluid flow transitions.

The understanding of the flow characteristics of PFPF from the viewpoint of multiphase flow is very critical. Lemmens (2006) conducted experiments on single- and two-phase flow through the globe valve and gave the clue that the pressure drop through the valve increased with the increase in void fraction. Chikhi (2016) suggested some methods to determine the void fraction and pressure drop for two-phase flow through the porous media and introduced the interfacial drag term to calculate the interfacial friction between the phases. Alimonti (2014) recommended the Chisholm model and the Lockhart-Martinelli model to predict pressure drops in two-phase flow in the globe valve and ball valve, respectively. The mass flow rate through a safety relief valve was predicted satisfactorily using the Homogeneous Equilibrium Model (HEM) (Dempster et al., 2013). The results indicated that the HEM method gave a good prediction for liquid mass fractions up to 0.4. Dinaryanto et al. (2017) investigated several basic mechanisms of slug flow by visual observation and pressure fluctuation measurement. They proposed a flow initiation map to address wave coalescences, wave growth mechanisms, and large disturbance waves.

The present work aims to study the bubble formation and the flow characteristics in the globe valve with a PFPF. The shadowgraph imaging technique was implied to illustrate the flow through the transparent valve model. This paper provides an understanding of pressure behavior inside the pipeline along with the globe valve and the characteristics of flow coefficient for varying conditions.

2. Experimental facility and procedure

2.1. Experimental setup

The two-phase (air-water) flow loop at Pusan National University is shown in Fig. 1. This loop consists of a reservoir tank, pump, flow meter, and the test section with a 3-inch nominal diameter pipeline and a total length of 18 m. The flow rate for the flow loop was generated by a multi-stage centrifugal pump with a maximum pump speed of 3500 RPM. Table 1 summarizes the specification of the facilities.

The test section is made of a 4-m length acrylic pipe to aid the visualization study. A series of nine Kistler 4043A2 piezo-resistive pressure gauges were equally spaced along the bottom of the pipeline from the upstream to the downstream of the valve (Fig. 2).

Table 1
Specification of flow loop test facilities.

Reservoir tank	Net volume of $2m^3$
Pump	5.5 kW h, Motor speed: 0–3500 RPM
Total length	18 m, stainless steel pipe
Test section	4 m, acrylic plastic pipe
Pipe diameter	3″

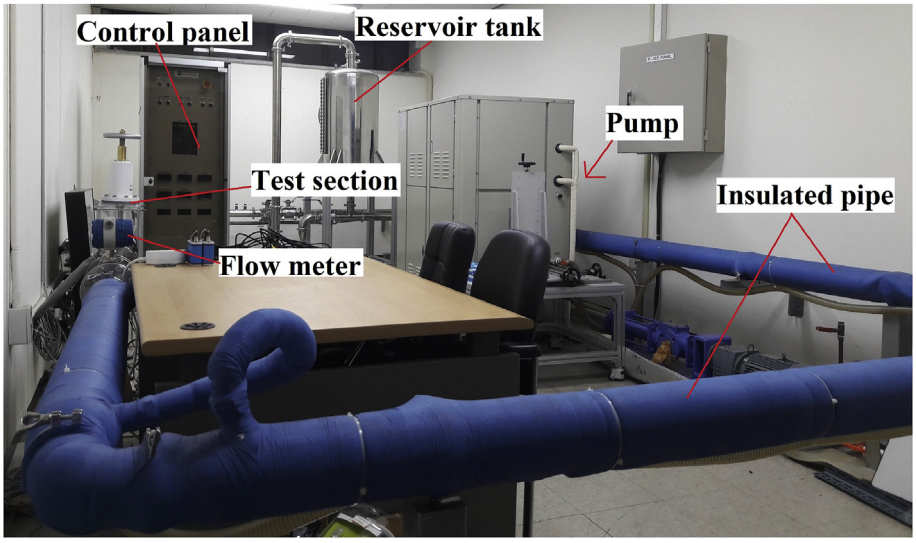

Fig. 1. Two-phase (air-water) flow loop in Pusan National University.

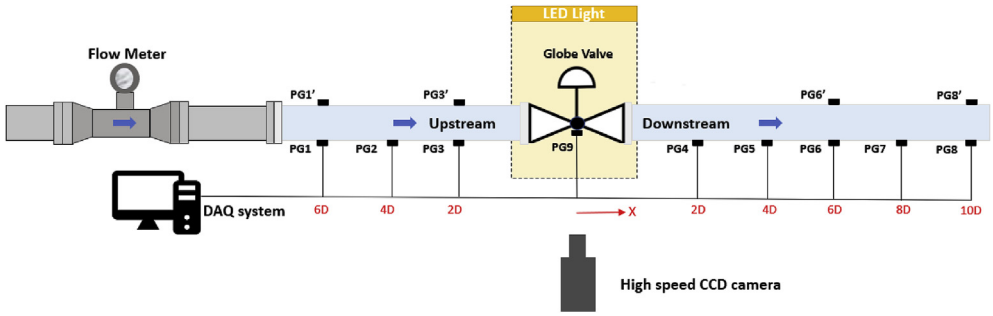

Fig. 2. Schematic of the test section.

Table 2
Specification of the pressure sensor and flow meter.

	Pressure sensor	Flowmeter
Sensor	KISTLER 4043A2	KTV-700
Type	Piezo-resistive	Vortex
Range	0–2 bar (abs)	2-100 (m^3/h)
Sampling rate	1000 Hz	50 Hz

Besides, four pressure gauges were installed on the top of the pipeline to investigate the difference in pressure between the top and the bottom of the pipe at the same cross-sections. Note that the PG3 at 2D inlet and PG6 at 6D outlet are the pressure tap positions recommended by the ANSI/ISA-75.01 standard (ISA, 2012).

A vortex-type flow meter was installed 10D away from the valve inlet. The specifications of the pressure sensor and the flow meter are listed in Table 2. The pressure and flow rate were obtained in 5 min of measurement, and there was 1 min of relaxation time for the stable measurements after the valve opening and pump speed change.

The valve model used in the experiment is a straight pattern (Z-shaped body) globe valve which has a nominal diameter of 3 inches and maximum valve travel of 5 cm. This is a prototype of an 8-inch sized globe valve designed according to ANSI B16.11 - Class 2500#, which has a scale ratio of 2.7:1 (Fig. 3). The globe valve prototype was tested at various valve openings which indicate how far the valve plug was moved relative to its maximum travel (Davis and Stewart, 2002).

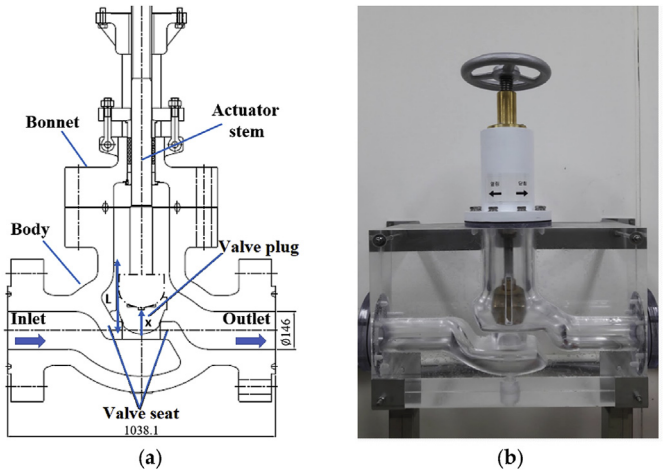

Fig. 3. Testing valve: (a) Design of an 8-inch globe valve according to ANSI B16.11 - Class 2500# globe valve; (b) 3-inch testing prototype.

$$\text{Valve opening } (\%), \alpha = \frac{x}{L} \times 100\% \quad (1)$$

where x denotes the valve travel from the fully closed position, and L means the maximum valve plug travel length (Fig. 3a). The valve opening was in increments of ten percent and ranged from 10% to 100%.

2.2. Shadowgraph imaging technique

The shadowgraph imaging technique was used to investigate fully filled and partially filled pipe flow (Fig. 4). To observe the formation of bubbles and the aerated flow inside the valve, a high-speed CCD camera (Redlake Y5) was used. The camera was equipped with a 105-mm, f/1.8 macro focal lens set at f/2.8 and the images were obtained with a maximum frame rate of 500 fps. Several LED lamps were used as lighting sources to support the visualization study. The detailed specification of the camera is shown in Table 3 below.

2.3. Experimental conditions

The experimental tests were carried out with 100% (fully filled) and 90% (partially filled) volume Water Fraction (WF) in the pipeline (Table 4). To establish practically the 100% WF flow, the pipeline and the reservoir tank were fully filled, and the flow circulation was generated by the pump gradually from slow to fast velocity to diminish every air component exist in the pipeline. With the assumption that the pipeline was ideally horizontal, the 90% WF was determined as the ratio of the flow area A_l occupied by the water over the cross-section area A of the pipe. Fig. 5 shows the WF measurement and Eqs. (2) and (3) give details of the calculation.

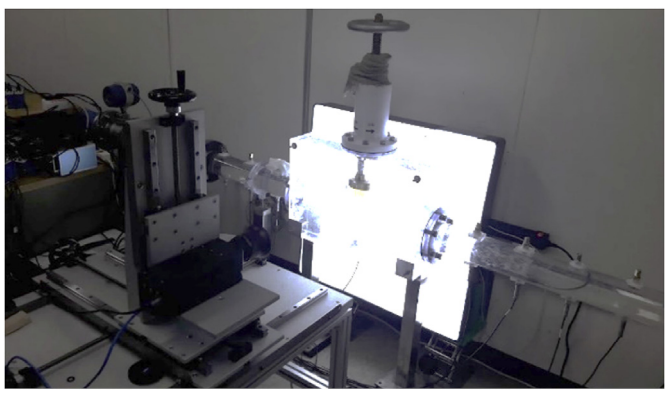

Fig. 4. Shadowgraph imaging technique.

Table 3
Specification of the high-speed CCD camera.

Maximum resolution	2352 × 1728 pixels
Pixel size	7 μm
Dynamic range	8 bit
Acquisition rate	500 Hz
FOV	495 × 364 mm^2

Table 4
Experimental conditions for measurement of flow coefficients.

Valve opening	Water fraction	Pump Speed
10–100% (every 10%)	100% 90%	1000–2000 rpm (every 100 rpm)

With the known pipe radius and the measured water column height from the shadowgraph image, the WF could be calculated.

$$WF = \frac{A_l}{A} = \frac{(\theta - sin\theta cos\theta)}{\pi} \tag{2}$$

$$cos\theta = \frac{R-d}{R} \tag{3}$$

The test was to investigate the flow coefficient, which describes the relationship between pressure drop and flow rate through the valve at each valve opening:

$$K_v = Q\sqrt{\frac{SG}{\Delta P}} \tag{4}$$

where Q and ΔP are the flow rate and the pressure drop through the valve, respectively; SG is the specific gravity of the liquid being measured to water (SG = 0.9982 in this study). The pressure drop was measured between pressure gauges PG3 and PG6 which are 2D from the upstream and 6D from the downstream of the valve (Fig. 2). Eq. (4) is used for single, incompressible, and turbulent flow without cavitation and choked in the valve, which satisfies the conditions in this study. To date, there is no standard formula exist for the calculation of the flow coefficient in two-phase flow through the control valve. Based on the experience and the available literature, Parcol valve manufacturer (2016) suggested a formula to determine K_v in two-phase flow without mass and energy transfer between the phases. The expression of K_v for separated gas-liquid flow with low volume fractions of the gas phase is as Eq. (5).

$$K_v = K_{v.l} + K_{v.g} \tag{5}$$

where $K_{v.l}$ and $K_{v.g}$ are the independent calculation of flow coefficients for the liquid phase and the gaseous phase, assuming that the mean velocities of the two phases are considerably different. This assumption may be acceptable for this experimental condition, where the air velocity is assumed to be zero.

3. Results and discussion

3.1. Bubble formation

Visualization studies were carried out at every 10 degrees of opening in 100% and 90% WF flow (Fig. 6 and Fig. 7). The present study focuses on the characterization of the flow inside the globe valve. (The video version of these figures is available in the online version of this article). The flow in 100% WF showed no exceptional incidents where the flow was nearly ideally stable at every valve opening without any bubbles. However, in the case of 90% WF, there were great quantities of bubbles formed at the valve throat and resulted in vortices in the valve chamber. The three-dimension-aerated flow produced shaking and a slight noise at the valve before passing to the downstream pipe section.

Fig. 8 and Fig. 9 are the snapshots of the flow with 90% WF at upstream and downstream, respectively. Fig. 8 illustrates the form of slug flow with roll waves and the free-surface deformation in the valve upstream. After the interaction with the globe valve, plumes of bubbles are created, and the highly aerated flow arises throughout a long pipe section downstream (Fig. 9).

The air entrainment process and self-aerated flow in the globe valve in the WF of 90% are shown in detail in Fig. 10. In PFPF, the large waves appeared in the form of roll waves in the valve upstream and produced complexity of air-water interactions. At the pipe bends (point 1 in Fig. 10), the free air was entrapped, and the bubbles were formed due to the sudden change in direction and the collision for flow with the pipe wall. The bubbles coalesced and produced vortices after the entrainment region. The aerated flow then hits the valve plug and changes its direction again at the vena contracta. As a result, the large bubbles were broken into a cloud of the aerated tiny bubble and to prolong in the valve downstream.

3.2. Pressure characteristics

The pressures were measured on the wall of the pipeline from 6D inlet to 10D outlet of the valve and the pressure magnitudes

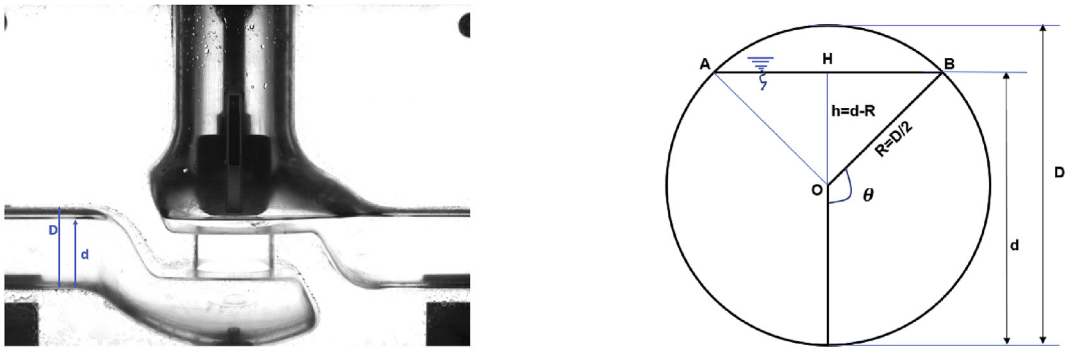

Fig. 5. WF measurement: (a) Water column measurement; (b) Cross-section of the pipe.

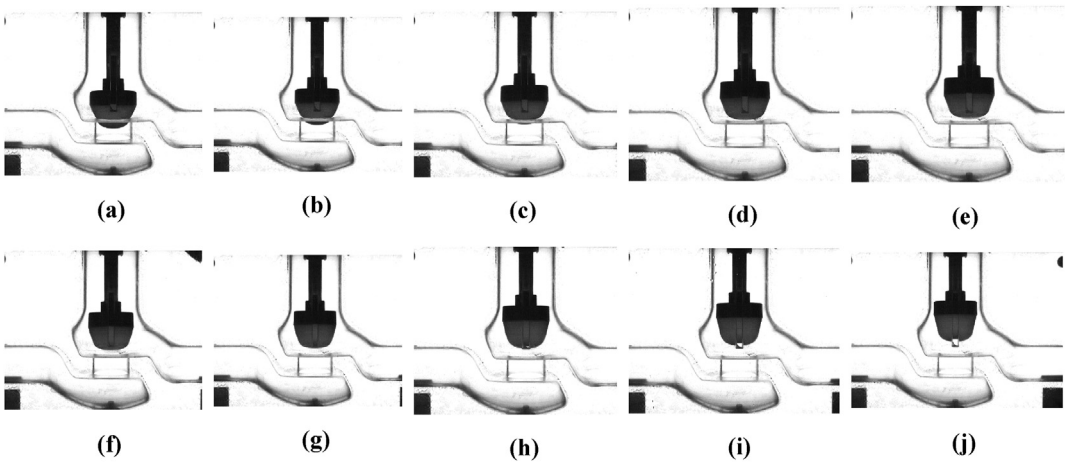

Fig. 6. Flow visualization inside the globe valve in 100% WF: a) 10% opening. (b) 20% opening. (c) 30% opening. (d) 40% opening. (e) 50% opening. (f) 60% opening. (g) 70% opening. (h) 80% opening. (i) 90% opening. (j) 100% opening.

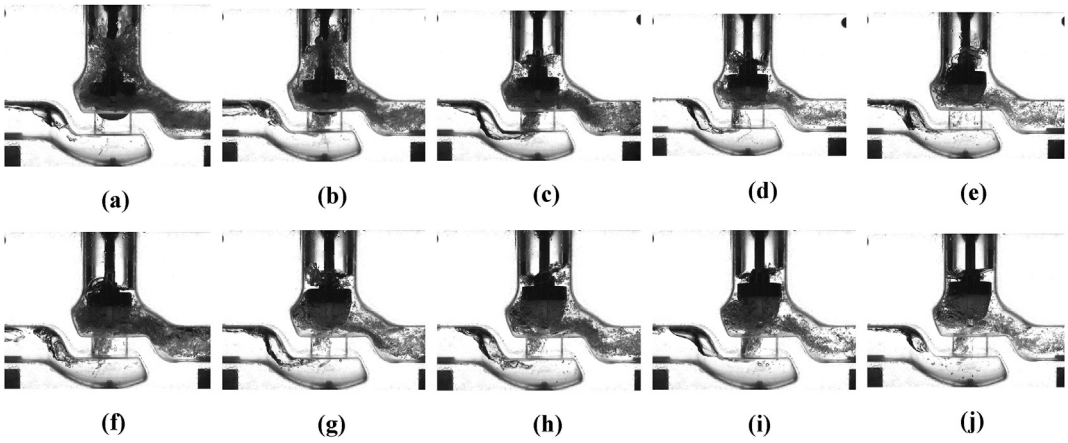

Fig. 7. Flow visualization inside the globe valve in 90% WF: a) 10% opening. (b) 20% opening. (c) 30% opening. (d) 40% opening. (e) 50% opening. (f) 60% opening. (g) 70% opening. (h) 80% opening. (i) 90% opening. (j) 100% opening.

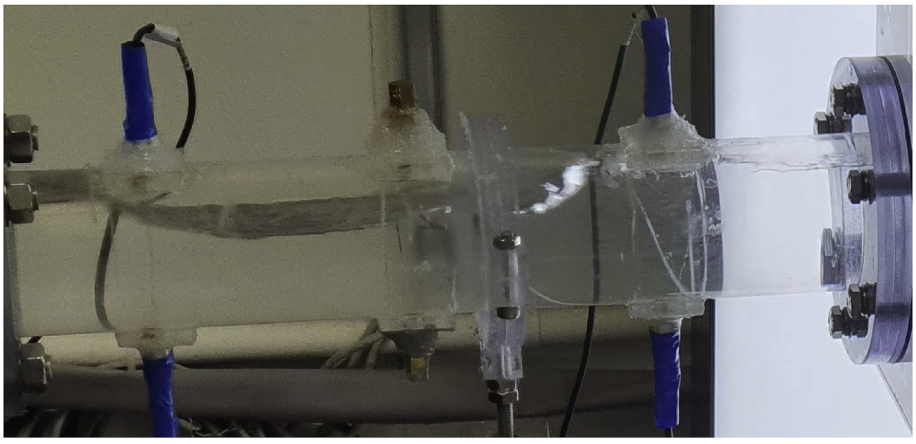

Fig. 8. Snapshot of the flow at the valve upstream.

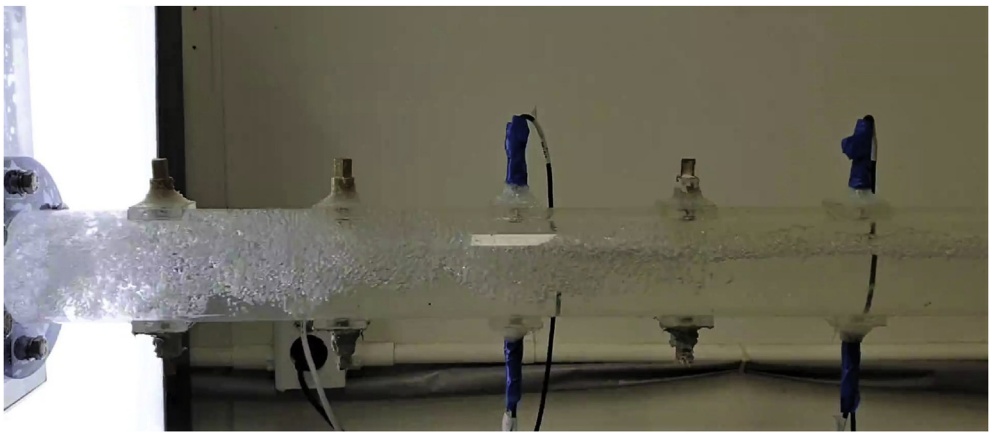

Fig. 9. Snapshot of the flow at the valve downstream.

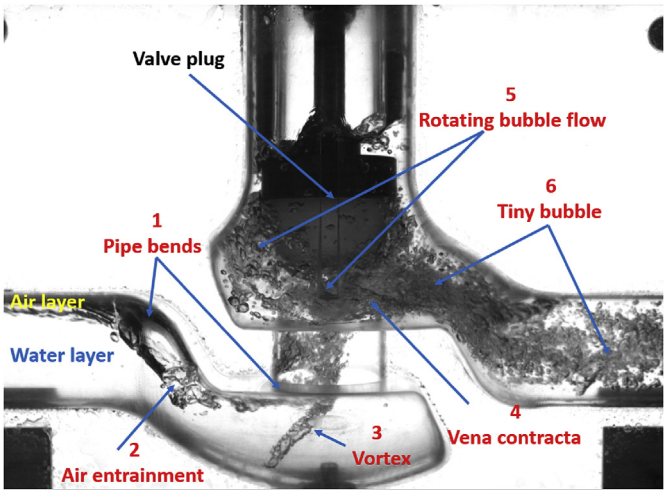

Fig. 10. Bubble formation in globe valve in 90% WF flow.

with their standard deviations are shown in Fig. 11. The measurement showed a continuous decreasing pressure with the increase in the valve opening from 10% to 50% before leveling off with further openings, which represented a quick-opening characteristic valve (Nguyen et al., 2020). Significant large pressures are obtained with the small valve openings at 10% and 20% (Fig. 11a and b). The very narrow flow path between the valve plug and valve seat might stifle the flow. For that reason, valve manufacturers usually recommend not to operate the valve with a valve opening smaller than 20% (Bauman, 2009; Monsen, 2013). For each opening, the pressures begin to drop when the fluid passed through the valve (X/D = 0) and show similar values for different locations along with the upstream (from −6 of X/D to −2) and downstream of the valve (from 2 of X/D to 10).

In 90% WF, the pressure drops undergo a decrease in magnitude compared to those in the fully filled flow (Fig. 12). Nevertheless, the line graphs in both cases confirm the quick-opening characteristics of the valve. Fig. 13 deduces the ratio of pressure drops (Φ) in 100% WF to 90% WF. At a specific valve opening, the ratios increase linearly with the Reynolds number (Fig. 13a). The differences at 10% valve opening are notable where the pressure drops in 100% WF are 1.6–3.4 times higher than those in 90% WF. The ratios decrease significantly at 20% opening and show almost similar values for further increase in valve opening. Table 5 summarizes the linear fitting parameters for each valve opening. Besides, the ratios grow faster with smaller valve openings and level off from 30% valve opening, for the same increase in Reynolds number. This is displayed by the slopes of the linear trendlines (m_Φ) in Fig. 13b.

The ANSI/ISA-75.01 standard (ISA, 2012) recommended tapping the pressure gauges at the 2D inlet and 6D outlet of the valve for pressure drop calculation. In this study, the comparison between measured pressures at different positions to the values at reference taps was conducted. From observation by shadowgraph images, there were a lot of bubbles appearing at the valve throat and downstream of the valve in PFPF. This may have a link with the difference in pressure between the bottom and the top of the pipeline at the same cross-sectional plane (Fig. 2).

Fig. 14 and Fig. 15 compare pressures at various pump speeds at upstream and downstream sides, respectively. In 100% WF flow, there are no remarkable differences between the pressures at various measurement locations with the recommended positions. The magnitude of the ratios is almost 1 for all valve openings and pump speeds. In the case of 90% WF, the pressures downstream of the valve show a considerable discrepancy between different positions. The ratio deflects well from the unity, especially at the small valve openings (Fig. 15). Fig. 16 also shows notable differences between pressures at the top and the bottom of the pipeline in PFPF, especially at the 6D outlet. The differences are significant at 10%, 20%, and 30% valve openings. Note that in the shadowgraph images (Figs. 6–10), the flow before the valve was as stable as in the single-phase water flow. However, when the flow passed through the valve, the air bubbles were generated, and the large recirculation region developed in the valve chamber and on the downstream side. At the small valve openings, bubble formation is severe due to the high resistance of the valve. The critical high local velocity of the bubble produces the differences in pressure distribution downstream of the valve. Therefore, it is recommended to have the minimum opening no less than 30% to provide stable operation for the globe valve in PFPF. In fact, the recommendation of 20% opening (Bauman, 2009; Monsen, 2013) is the most unstable condition (Fig. 15).

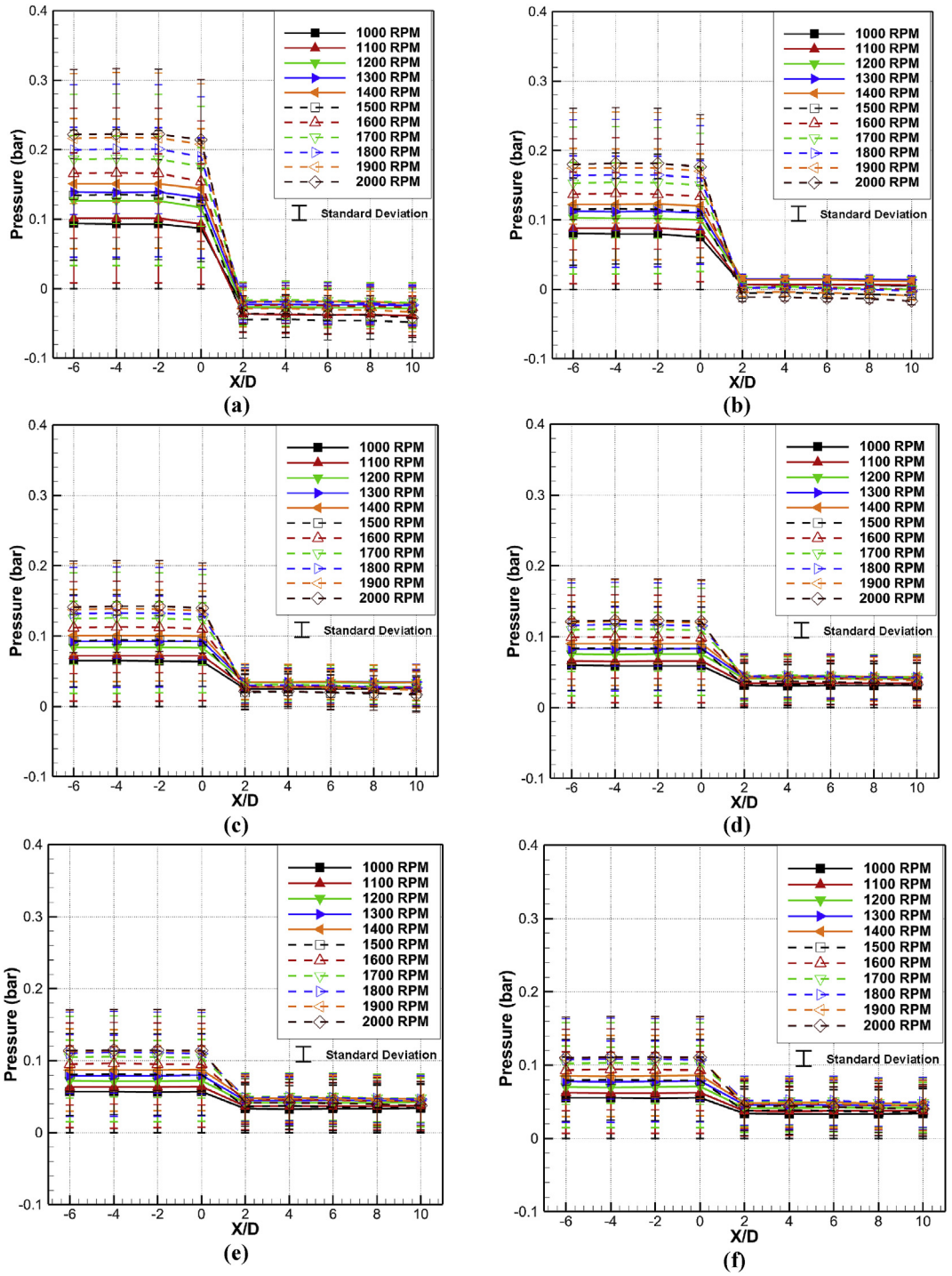

Fig. 11. Pressure distribution: (a) 10% opening. (b) 20% opening. (c) 30% opening. (d) 40% opening. (e) 50% opening. (f) 60% opening. (g) 70% opening. (h) 80% opening. (i) 90% opening. (j) 100% opening.

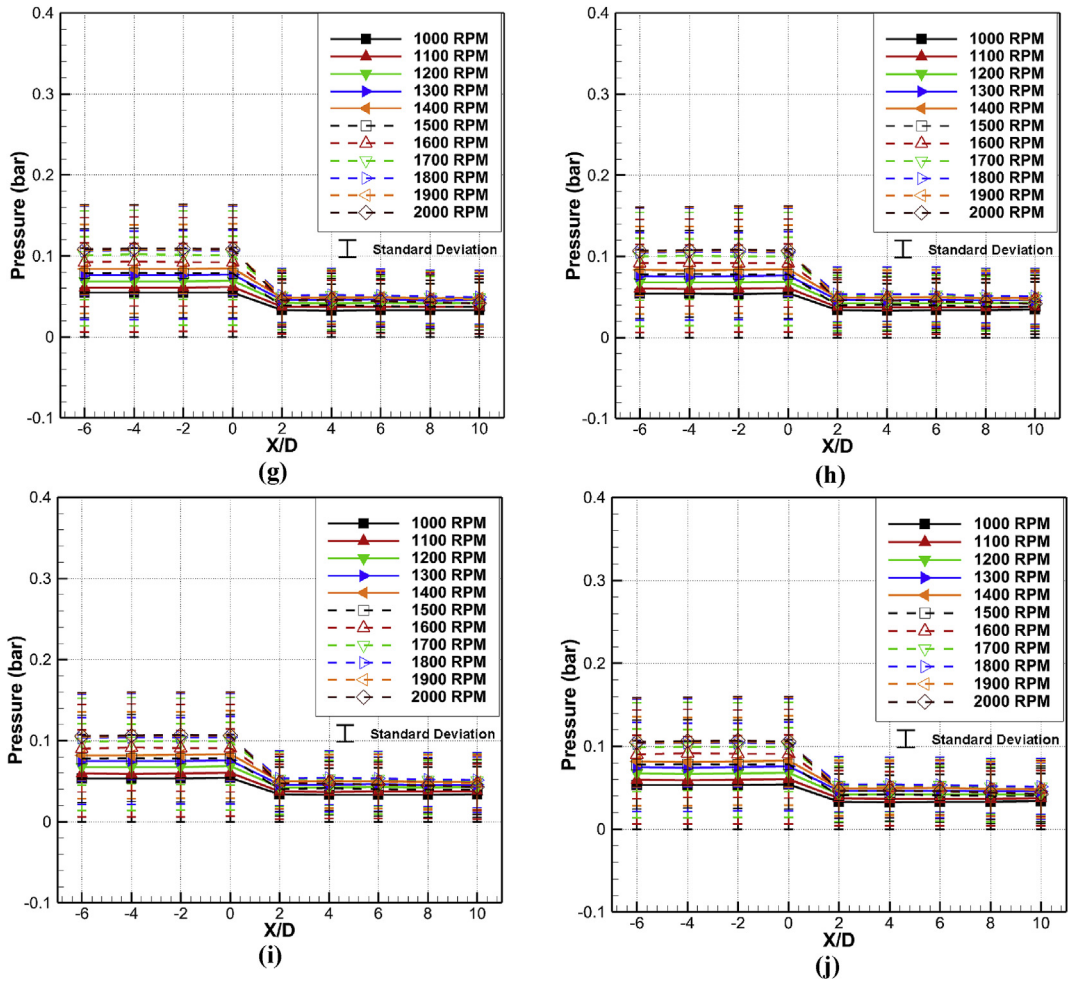

Fig. 11. (*continued*).

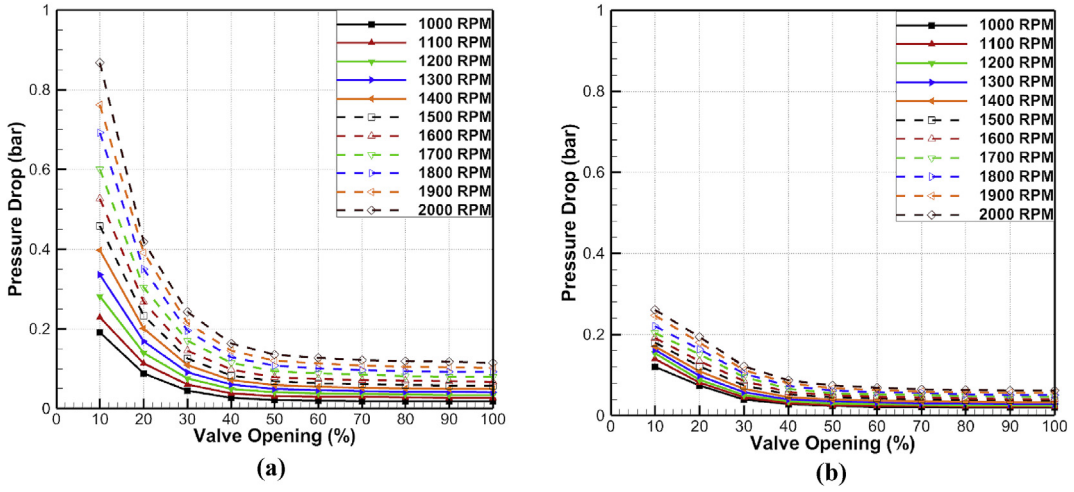

Fig. 12. Pressure drop at the globe valve: (a) 100% WF. (b) 90% WF.

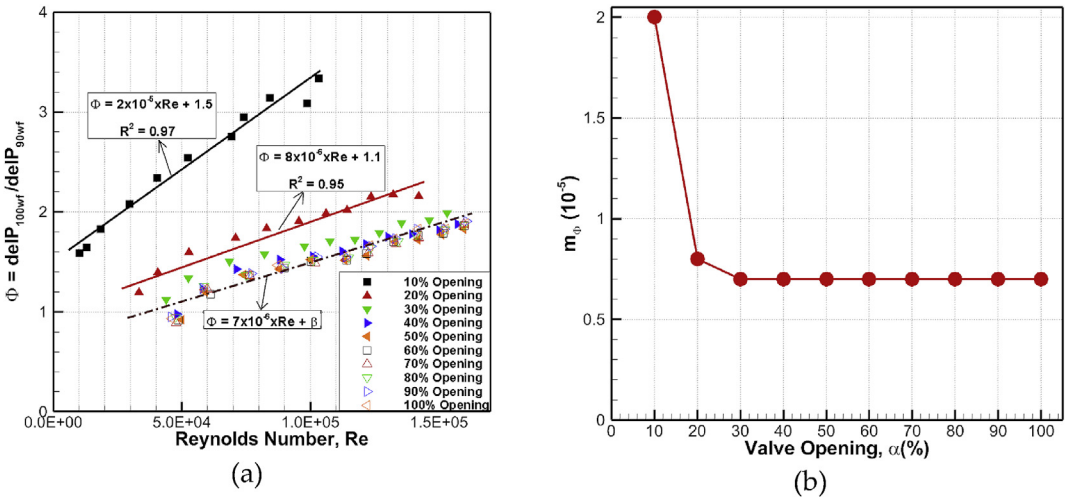

Fig. 13. Pressure drop deduction: (a) ratios of pressure drop in 100% WF to 90% WF; (b) reduction of the pressure drop ratio for the same increase in Reynolds number.

Table 5
Fitting parameters for the linear trendlines of pressure drop ratio (Φ) to Re

Valve Opening, α	Reduction of Φ, m_Φ	β	R^2
10	2×10^{-5}	1.5	0.97
20	0.8×10^{-5}	1.1	0.95
30	0.7×10^{-5}	1.0	0.95
40	0.7×10^{-5}	0.8	0.92
50	0.7×10^{-5}	0.8	0.92
60	0.7×10^{-5}	0.8	0.92
70	0.7×10^{-5}	0.7	0.93
80	0.7×10^{-5}	0.8	0.94
90	0.7×10^{-5}	0.7	0.96
100	0.7×10^{-5}	0.7	0.95

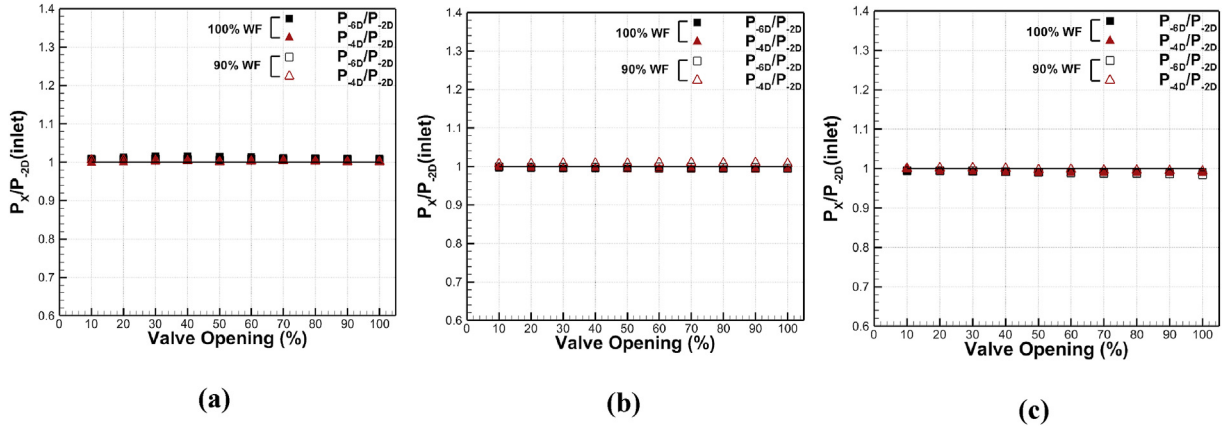

Fig. 14. Comparison of pressure at the valve upstream: (a)1000 RPM; (b) 1500 RPM; (c) 2000 RPM.

3.3. Flow coefficient

In PFPF, it is assumed that the flow rate of the air existing on the top part of the pipeline is zero. Therefore, the contribution of the air on the calculation of the total flow coefficient in Eq. (4) might be negligible. However, the effect of the air on flow coefficient is demonstrated by its effects on pressure drop (Fig. 12) and the flow rate (Fig. 17), which are involved in flow coefficient calculation. Fig. 18 compares the flow coefficients in 100% WF and 90% WF pipe flows. For small pump speeds, the flow coefficients of the 90% WF

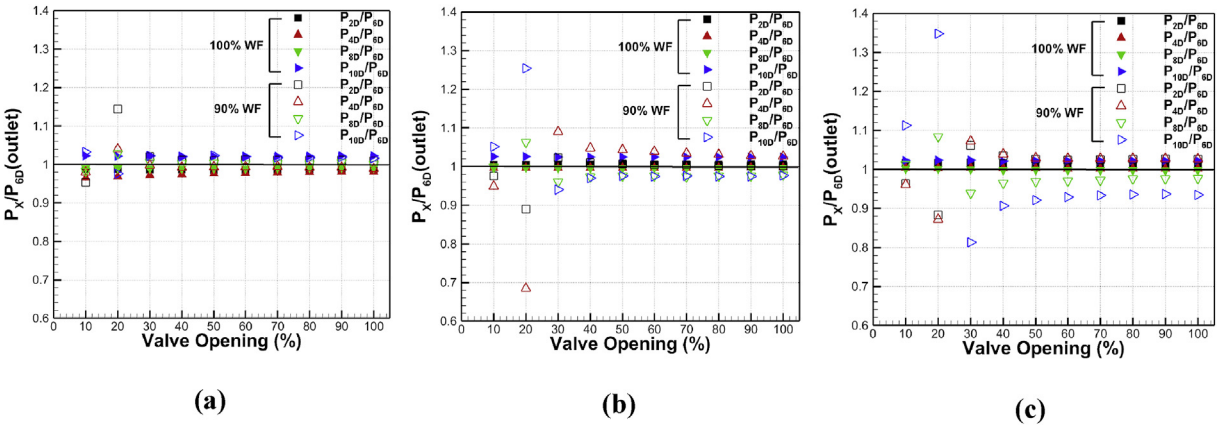

Fig. 15. Comparison of pressure at the valve downstream: (a) 1000 RPM; (b) 1500 RPM; (c) 2000 RPM.

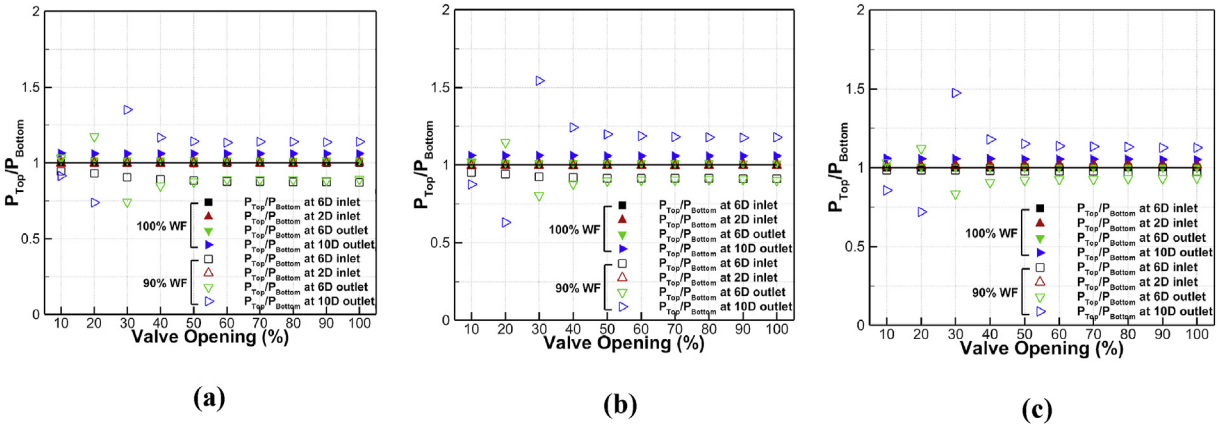

Fig. 16. Comparison of pressure at the top to the bottom of the pipeline: (a) 1000 RPM; (b) 1500 RPM; (c) 2000 RPM.

flow are much lower than those of 100% WF flow because the flow rates are lower while the pressure drops are consistent. For high pump speeds (>1600 RPM), the rate of decrease in pressure drop in the case of 90% WF is greater than the rate of decrease in flow rate Q, which follows in larger flow coefficients. Nevertheless, the flow coefficients in both cases show the same quick-opening characteristics, although there were fluctuations in the 90% WF flow coefficient due to the bubble effect.

In addition, the flow coefficients of 90% WF show no convergence characteristics with the Reynolds number as found in the case of 100% WF (Nguyen et al., 2020) Alternatively, they increase linearly with Re at every valve opening (Fig. 19a). Table 6 shows all

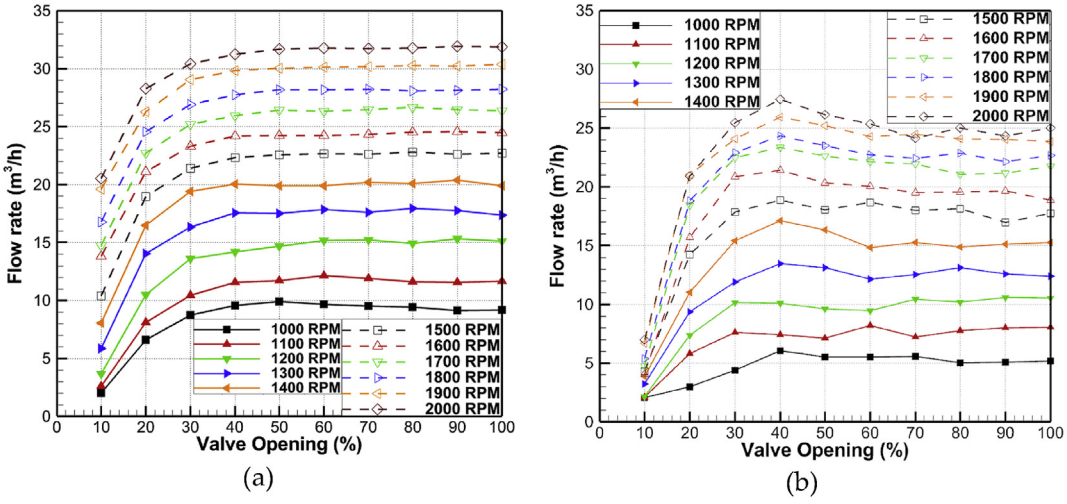

Fig. 17. Flow rate of the globe valve: (a) 100% WF; (b) 90% WF.

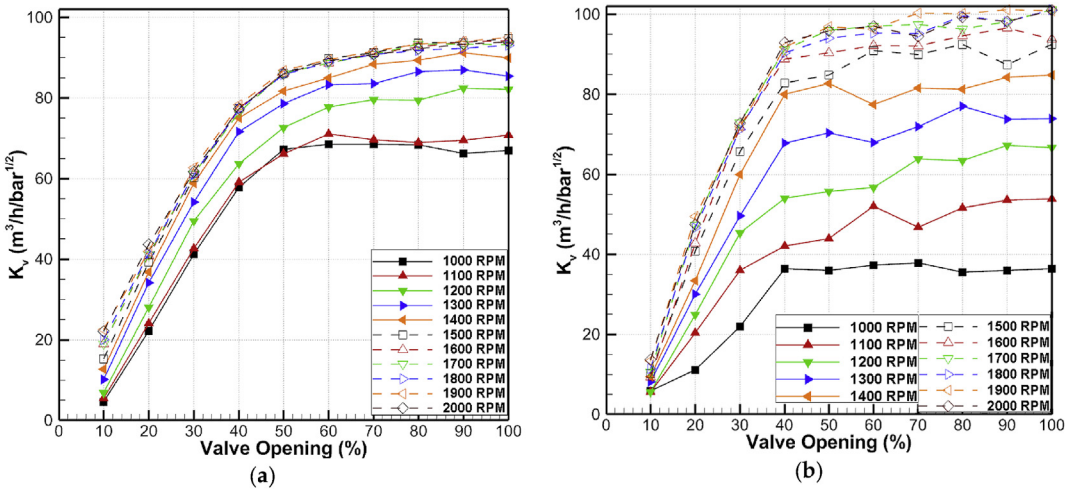

Fig. 18. Flow coefficient of the globe valve: (a) 100% WF; (b) 90% WF.

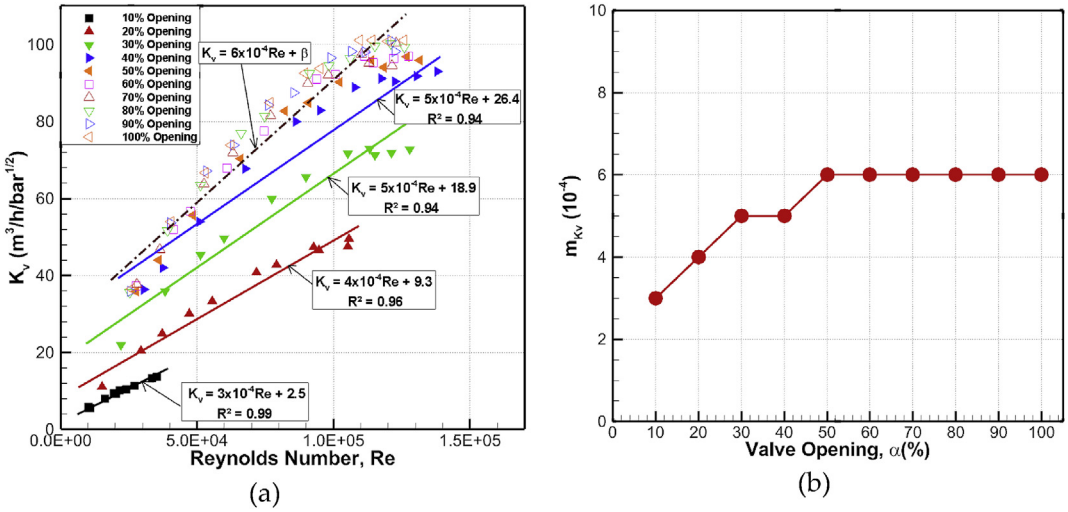

Fig. 19. 90% WF flow coefficient deduction: (a) flow coefficients increase linearly with Re; (b) increment of flow coefficient for the same increase in Reynolds number.

fitting parameters for each valve opening. The increment of flow coefficients to valve opening is represented by the slope of linear trendlines (m_{Kv}), which increase continually and level off at 50% degree of opening (Fig. 19b). In another word, the flow coefficient of the glove valve grows faster with large valve openings before being stable at 50% opening, for the same increase in Reynolds number.

Table 6
Fitting parameters for the linear trendlines of K_v to Re

Valve Opening, α	Increment of K_v m_{Kv}	β	R^2
10	3×10^{-4}	2.5	0.99
20	4×10^{-4}	9.3	0.96
30	5×10^{-4}	18.9	0.94
40	6×10^{-4}	26.4	0.94
50	6×10^{-4}	26.6	0.94
60	6×10^{-4}	28.2	0.95
70	6×10^{-4}	28.4	0.94
80	6×10^{-4}	29.4	0.93
90	6×10^{-4}	30.0	0.93
100	6×10^{-4}	30.2	0.93

4. Conclusions

An experimental study on PFPF in a horizontal, transparent pipe of 3-inch nominal diameter has been conducted. The study focuses on the formation of bubbles and the effect of aerated flow on pressure characteristics and flow coefficient of the globe valve. The visualization study was employed with the shadowgraph imaging technique to investigate bubble formation in the globe valve. The pressure distribution along the pipeline upstream and downstream of the test valve was measured and the flow coefficients were determined. The results indicate that:

1. The free air in the pipeline can be accumulated and entrained to form the bubble at the bends of the globe valve. There is a coalescence of the formed single bubble and the large aerated flow is then collapsed into a dense plume of the bubble at the vena contracta of the valve.
2. In PFPF, the pressures downstream of the valve show a considerable discrepancy between the locations, especially in valve openings smaller than 30%. As a result of the complex rotational flow with a lot of bubbles occurring inside of the valve and passing on the valve downstream, the differences are expected.

The pressure drops of the valve in 90% WF are much lower than those of 100% WF flow, which is up to 3.5 times at the smallest degree of valve opening. The rate of the decrease in pressure drops enlarge with smaller valve openings and level off from 30% valve opening, for the same increase in Reynolds number. In PFPF, thus, it is recommended to operate the globe valve with an opening of no less than 30% to have a stable control and avoid any possible damage.

3. The flow coefficients in PFPF show the same quick-opening characteristics as those in fully filled flow despite the fluctuation caused by the effect of air bubbles. Besides, the flow coefficients increase linearly with the Reynolds number. For the same increase in Re, the flow coefficients increase continually with valve openings and become stable from 50% of the opening.

Declaration of competing interest

The authors declare that they have no known competing financial interests or personal relationships that could have appeared to influence the work reported in this paper.

Acknowledgments

This work was supported by the R&D Platform Establishment of Eco-Friendly Hydrogen Propulsion Ship Program (No. 20006636) and Global Advanced Engineer Education Program for Future Ocean Structures (P0012646), funded by the Ministry of Trade, Industry and Energy.

Appendix A. Supplementary data

Supplementary data to this article can be found online at https://doi.org/10.1016/j.ijnaoe.2021.06.007.

References

Alimonti, C., 2014. Experimental characterization of globe and gate valves in vertical gas-liquid flows. Exp. Therm. Fluid Sci. 54, 259–266. https://doi.org/10.1016/j.expthermflusci.2014.01.001.

Bauman, H.D., 2009. Control Valve Primer: A User's Guide, fourth ed. ISA Research Triangle Park, Durham, NC, USA, pp. 53–61.

Chatterjee, S., Sugilal, G., Prabhu, S.V., 2017. Heat transfer in a partially filled rotating pipe with single phase flow. Exp. Therm. Fluid Sci. 83, 47–56. https://doi.org/10.1016/j.ijthermalsci.2017.11.024.

Chatterjee, S., Sugilal, G., Prabhu, S.V., 2018. Flow transitions in a partially filled rotating inclined pipe with continuous flow. Int. J. Therm. Sci. 125, 132–141. https://doi.org/10.1016/j.expthermflusci.2016.12.007.

Chikhi, N., Clavier, R., Laurent, J.-P., Fichot, F., Quintard, M., 2016. Pressure drop and average void fraction measurements for two-phase flow through highly permeable porous media. Ann. Nucl. Energy. https://doi.org/10.1016/j.anucene.2016.04.007.

Davis, J.A., Stewart, M., 2002a. Predicting globe control valve performance—Part I: CFD modeling. J. Fluid Eng. 124 (3), 772–777. https://doi.org/10.1115/1.1490108.

Davis, J.A., Stewart, M., 2002b. Predicting globe control valve performance—Part II: experimental verification. J. Fluid Eng. 124 (3), 778–783. https://doi.org/10.1115/1.1490126.

Dempster, W., Elmayyal, W., 2013. Two-phase discharge flow prediction in safety valves. Int. J. Pres. Ves. Pip. 110, 61–65. https://doi.org/10.1016/j.ijpvp.2013.04.023.

Dinaryanto, O., Prayitno, Y.A.K., Majid, A.I., Hudaya, A.Z., Nusirwan, Y.A., Widyaparaga, A., Indarto, Deendarlianto, 2017. Experimental investigation on the initiation and flow development of gas-liquid slug two-phase flow in a horizontal pipe. Exp. Therm. Fluid Sci. 81, 93–108. https://doi.org/10.1016/j.expthermflusci.2016.10.013.

Ferreira, J.P.B.C.C., Martins, N.M.C., Covas, D.I.D., 2018. Ball valve behavior under steady and unsteady conditions. J. Hydraul. Eng. 144 (4) https://doi.org/10.1061/(ASCE)HY.1943-7900.0001434.

Grace, A., Frawley, P., 2011. Experimental parametric equation for the prediction of valve coefficient (Cv) for choke valve trims. Int. J. Press. Vessel. (88), 109–118. https://doi.org/10.1016/j.ijpvp.2010.11.002.

Henry, C.-H. Ng, Cregan, H.L.F., Dodds, J.M., Poole, R.J., Dennis, D.J.C., 2018. Partially filled pipes: experiments in laminar and turbulent flow. J. Fluid Mech. 848, 467–507. https://doi.org/10.1017/jfm.2018.34.

Instrument Society of America, 1972. Control Valve Sizing Equations for Incompressible Flow. ISA-S39.1 Standard, Research Triangle Park: Durham, NC, USA.

International Society of Automation, 2012. Flow Capacity – Sizing Equations for Fluid Flow under Installed Conditions. ANSI/ISA-75.01.01-2012 standard, Research Triangle Park: Durham, NC, USA.

Lemmens, M.H.M., 2006. Single- and Two-phase Flow through a Globe Valve: Experiments and Numerical Simulations. Master Internship Project, Roma, Italy.

Monsen, J., 2013. Control Valve Application Technology: Techniques and Considerations for Properly Selecting the Right Control Valve, first ed. Valin Corporation, San Jose, CA, USA, pp. 17–32.

Ng, T.S., Lawrence, C.J., Hewitt, G.F., 2001. Gravity-driven laminar flow in a partially - filled pipe. Chem. Eng. Res. Des. 79, 499–511. https://doi.org/10.1205/026387601750282445.

Nguyen, Q.K., Jung, K.H., Lee, G.N., Suh, S.B., To, P., 2020. Experimental study on pressure distribution and flow coefficient of globe valve. Processes 8, 875. https://doi.org/10.3390/pr8070875.

Parcol valve manufacturer, 2016. Handbook for Control Valve Sizing. Koso Parcol, Canegrate Mi, Italy.

Rahmeyer, W., Driskell, L., 1985. Control valve flow coefficients. J. Transport. Eng. 111, 358–364. https://doi.org/10.1061/(ASCE)0733-947X(1985)111:4(358).